Journal of Chemistry Studies
ISSN: 2753-4634
DOI: 10.32996/jcs
Journal Homepage: www.al-kindipublisher.com/index.php/jcs

JCS
AL-KINDI CENTER FOR RESEARCH AND DEVELOPMENT

| RESEARCH ARTICLE

Synthesis of Silver Nanoparticles Loaded with Tetracycline and Evaluation of Their Antibacterial Properties

Sayad Amiry [1] ✉, Mohammad Qasem Amini[2], Shafiq Ahmad Kahdestani [3] and Abul Khalil Kahdistani[4]
[134]*Department of Chemistry, Education Faculty of Herat University, Herat, Afghanistan*
[2]*Department of Biology, Faculty of Science, Herat University, Herat, Afghanistan*
Corresponding Author: Sayad Amiry, **E-mail**: sayad_amiry@yahoo.com

| ABSTRACT
Silver nanoparticles (AgNPs) synthesized using plant extracts exhibit promising medical applications. In this study, silver nanoparticles were synthesized from silver nitrate in the presence of iris flower extract, in which various parts of the plant—including leaves, roots, seeds, stems, and fruits—rich in antioxidants, were employed for the biosynthesis of silver nanoparticles. Tetracycline (Tetra) was subsequently loaded onto the surface of the silver nanoparticles to produce the Tetra–AgNP nanocomposite. The structural and morphological features of the Tetra–AgNP nanocomposite were characterized by X-ray diffraction (XRD), transmission electron microscopy (TEM), scanning electron microscopy (SEM), and Fourier-transform infrared spectroscopy (FT-IR). The crystalline nature of both the AgNPs and the Tetra–AgNP nanocomposites was confirmed by XRD analysis. FT-IR results demonstrated that the silver nanoparticles were coated with the plant extract and successfully loaded with the Tetra drug. TEM images revealed that the Tetra–AgNP nanocomposites exhibited an average particle size of 63.78 nm with a spherical morphology. SEM images confirmed a needle–aggregate morphology for both the AgNPs and Tetra–AgNPs. Furthermore, the cytotoxicity of AgNPs and Tetra–AgNP nanocomposites was evaluated using the normal DH5α cell line. The findings suggest that Tetra–AgNP nanocomposites are suitable candidates for drug delivery applications

| KEYWORDS
Silver nanoparticles, Iranian iris plant, green synthesis

| ARTICLE INFORMATION
ACCEPTED: 01 January 2026 **PUBLISHED:** 07 January 2026 **DOI:** 10.32996/jcs.2026.5.1.1

1. Introduction

In recent decades, nanotechnology and the application of various nanoparticle-based products have witnessed remarkable expansion across diverse industrial sectors [1]. In this regard, nanotechnology has entered the fields of medicine and pharmaceuticals, where it has been applied in prevention, diagnosis, and treatment. Scientific studies and reports indicate that the properties and activities of nanoparticles are directly related to their size, geometric shape, and type [2], [3]. Specifically, the smaller the nanoparticles, the more diverse and extraordinary their physicochemical and biological activities become [4].

Consequently, the production methods and the rate of application of nanomaterials in various morphologies—such as spherical, cubic, pyramidal, and needle-shaped—have rapidly expanded and are now employed in numerous aspects of life, including electronics, healthcare, antimicrobial control, disease diagnosis and treatment, pharmaceuticals, device manufacturing, biosensors, catalysts, textiles, and wastewater treatment [5]–[7]. Among the most significant applications of silver nanoparticles (AgNPs) today is their role in medicine and antimicrobial activity. Historically, metals and their compounds were used in pharmaceutical formulations. At present, however, metallic nanoparticles and their derivatives are utilized for purposes such as antimicrobials, insecticides, cosmetic and hygienic products, antibacterials, and various drugs with wide-ranging applications [8].

The production methods and broad applications of newly synthesized nanoparticles are regarded as innovative approaches in the chemical and pharmaceutical industries [9], [10]. Owing to their exceptional potential in environmental remediation,

Copyright: © 2026 the Author(s). This article is an open access article distributed under the terms and conditions of the Creative Commons Attribution (CC-BY) 4.0 license (https://creativecommons.org/licenses/by/4.0/). Published by Al-Kindi Centre for Research and Development, London, United Kingdom.

pharmaceutical production, and therapeutic processes, these nanoparticles are of great value in biological research, medical sciences, and drug delivery. For instance, some nanoparticles are reported to have the ability to destroy as many as 650 cancer cells in less than four hours [8], [11]–[13].

The incorporation of nanotechnology into essential oil formulations enhances their stability while simultaneously reducing toxicity and possible side effects [7]. Such compounds are also of significant value in environmental health, where they are applied to counteract soil, water, and air pollutants. For example, researchers at Shahrekord University of Medical Sciences demonstrated through an adsorption isotherm study that almond shells functionalized with magnetic iron nanoparticles effectively removed nitrate from aqueous environments [14].

One promising method for nanoparticle synthesis is nanophytosynthesis, in which the reduction of metal ions is mediated by plant-derived biomolecules—commonly referred to as secondary metabolites. Unlike conventional chemical and physical methods, this approach does not require toxic solvents or reagents, prolonged reaction times, high energy input, elevated temperature or pressure, or excessive costs [15], [16].

In the antibacterial activity of silver nanoparticles, particle size is a critical determinant. Recent studies have shown that silver nanoparticles interact with bacterial cell walls and cytoplasmic components, causing disruption of the cell wall structure, subsequent penetration into the cytoplasm, and eventual cell death [17]. Using Aloe vera extract, for example, spherical silver nanoparticles with an average size of 15.5 nm have been synthesized. In that method, the addition of ammonia to the reaction mixture facilitated the reduction of Ag^{+} ions to silver nanoparticles through the formation of a soluble complex [18]. The antibacterial activity of silver nanoparticle–plant composites synthesized from the leaves of Ocimum sanctum and Vitex negundo has been evaluated against Staphylococcus aureus, Vibrio cholerae, Proteus vulgaris, and Pseudomonas aeruginosa, with results reported across different concentrations [19].

Further investigations confirm that, overall, the antibacterial and antiviral activity of silver nanoparticles, ions, and composites is strongly influenced by their morphology and particle size, factors that directly determine their destructive potential [20]–[22]. Nonetheless, it must be noted that, alongside these benefits, nanoparticles may also pose risks of cytotoxicity to the tissues of living organisms [23].

In most antibacterial studies on nanocomposites, Escherichia coli, Staphylococcus aureus, Bacillus subtilis, and Staphylococcus epidermidis are commonly used as model microorganisms. Of these, E. coli and S. aureus are particularly important, as they are highly pathogenic and associated with a wide range of diseases. These bacteria are key agents of infections such as impetigo, skin infections, boils, abscesses, endocarditis, brain abscesses, and meningitis [24]. The emergence of antibiotic resistance in bacteria remains a major challenge to public health. In this context, nanoparticles with biological activity are considered promising candidates due to their high sensitivity in inhibiting or eradicating the growth and proliferation of pathogenic bacteria and viruses [25].

A scientifically plausible explanation for the biological activity of such nanomaterials, especially metallic nanoparticles, is their capacity to establish electrostatic interactions due to their surface charge (predominantly positive) and high surface-to-volume ratio. They can interact with proteins, enzymes, and microbial DNA through electron exchange with groups such as alcohols, amines, amides, carboxylates, thiols, indoles, and imidazoles, which generally carry partial negative charges. This interaction ultimately leads to microbial inactivation, though the immune response of the host organism must also be considered [26]–[28].

In the present study, given the challenge of bacterial resistance to antibiotics and the issues discussed above, silver nanoparticles were synthesized using the nanophytosynthesis approach with Iris persica extract. Tetracycline was used as a reference drug, and the enhancement of its antibacterial properties through silver nanoparticle conjugation was evaluated. The results demonstrate that the antibacterial activity of the synthesized AgNPs using plant extracts surpassed that of the extracts alone. Furthermore, silver nanoparticles synthesized using O. sanctum exhibited higher antibacterial activity compared with those derived from V. negundo. The tetracycline–silver nanocomposite synthesized via nanophytosynthesis proved capable of effectively destroying E. coli cells through cell wall disruption and lysis.

2. Methodology

In this study, the plant Iris persica (commonly known as the Persian iris or Nowruz flower) was used for the synthesis of silver nanoparticles. This plant is native to Iran and Afghanistan. It is a small species, approximately 10 cm in height, with leaves measuring 5–15 mm in width. Its flowers are about 5 cm long and occur in various colors, including brownish-gray, greenish, blue, and purple. For the purpose of this research, both the roots and aerial parts (stems, leaves, and flowers) of the plant were utilized in aqueous and alcoholic solutions. The experimental treatments applied in this study were as follows:

- A: Root extract with aqueous solvent
- B: Aerial parts extract with aqueous solvent

Figure 1. Image of the plant Iris persica (Persian iris) [29].

2.1 Extraction and Synthesis

For the extraction process, the aerial parts and roots of the plant were first dried separately under shade, away from light and heat. Subsequently, both the roots and aerial parts were ground to obtain a uniform powder.

Aqueous extract preparation:

To prepare the aqueous extract, 7–10 g of the plant powder was added to 100 mL of distilled water. The mixture was heated on a magnetic stirrer to ensure uniform mixing. Afterwards, the volume was adjusted by adding distilled water up to 150 mL, and the solution was boiled for 10 minutes. The mixture was then cooled and filtered using filter paper to remove any suspended or residual particles, yielding a clear solution. The filtrate was concentrated by rotary evaporation until approximately 80% of the solvent had evaporated. To this concentrated extract, 100 mL of triple-distilled deionized water, 0.196 g of silver nitrate, and 250 mg of tetracycline were added. The solution was stirred at 70 rpm for 4–6 hours until a visible color change to brown or black indicated nanoparticle formation.

Alcoholic extract preparation:

For the alcoholic extract, 7–10 g of plant powder was added to 250 mL of ethanol, and the container was covered with aluminum foil to prevent light exposure. The solution was placed on a rotary shaker at 70 rpm for 48 hours, during which it was filtered several times. The resulting extract was concentrated by rotary evaporation until approximately 80% of the solvent had evaporated, followed by multiple filtration steps. To synthesize nanoparticles, 6 mL of ethanol, 4 mL of the extract, 0.017 g of silver nitrate, and 250 mg of tetracycline were combined, and the reaction was allowed to proceed for 2 hours, during which a distinct color change was observed.

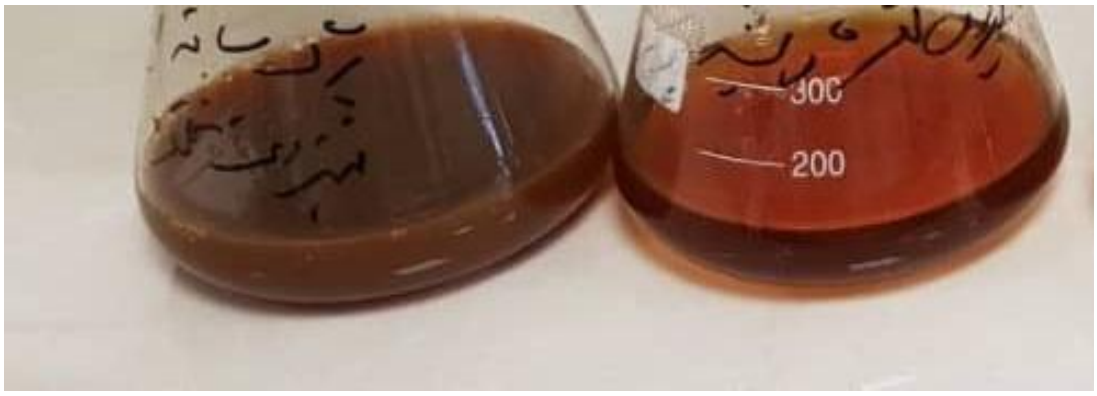

Figure 2. From right to left: (a) aqueous extract of root; (b) aqueous extract of stem and leaves.

2.2 Centrifugation of Samples

Following the measurement of optical density (OD) of the silver nitrate-containing solutions, the samples were subjected to centrifugation in four stages to obtain silver nanoparticle powder. In the first step, the solution was centrifuged directly at 1300 rpm for 20 minutes at 18 °C. The supernatant was carefully removed with a pipette, leaving a silver-saturated precipitate.

In the subsequent three stages, 10 mL of solution was added each time, followed by centrifugation and removal of the supernatant. In the final stage, the remaining saturated fraction was transferred into a watch glass and allowed to dry for two days. The dried

samples were then scraped with a sterile blade and transferred into sterile microtubes. The obtained nanoparticle powder did not require refrigeration for storage. The synthesized silver nanoparticles are shown in Figure 3.

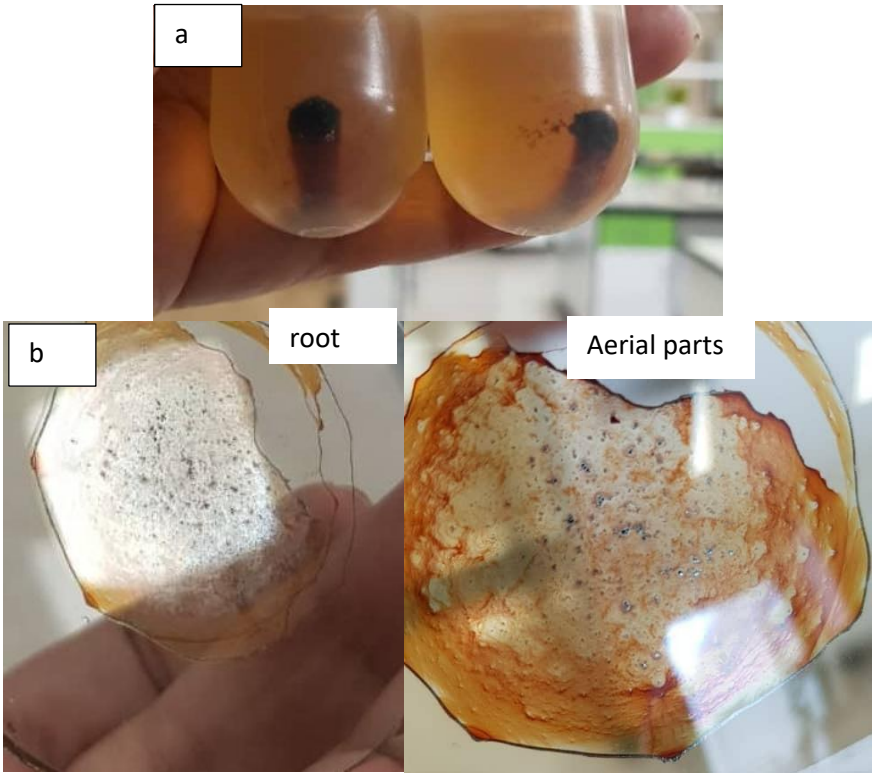

Figure 3. Images of silver nanoparticles synthesized using aqueous solutions: (a) after two centrifugation cycles; (b) precipitate obtained after four centrifugation cycles, dried on a watch glass for two days.

2.3 Preparation of Pure Extract

To prepare the pure extract, silver nitrate was not added. The crude extract is often prone to fungal contamination; therefore, rapid drying is required. For this purpose, a freeze-dryer was employed, with the aqueous solution cooled to –80 °C and the alcoholic solution to –100 °C

2.4 Cell and Tissue Culture

The viability of cells after 14 days of culture was assessed on culture plates in the presence of a sterile environment. To each well, 0.5 mL of DMEM culture medium and 50 µL of MTT solution (3-(4,5-dimethylthiazol-2-yl)-2,5-diphenyltetrazolium bromide, 5 mg/mL; Sigma-Aldrich) were added. After 4 hours of incubation, 0.5 mL of dimethyl sulfoxide (DMSO) was added to dissolve the formed formazan crystals. Following a 20-minute period, the absorbance of the cells/wells was measured at a wavelength of 570 nm using a microplate reader [2] (Figure 4).

Examining cell capabilities using the MTT test

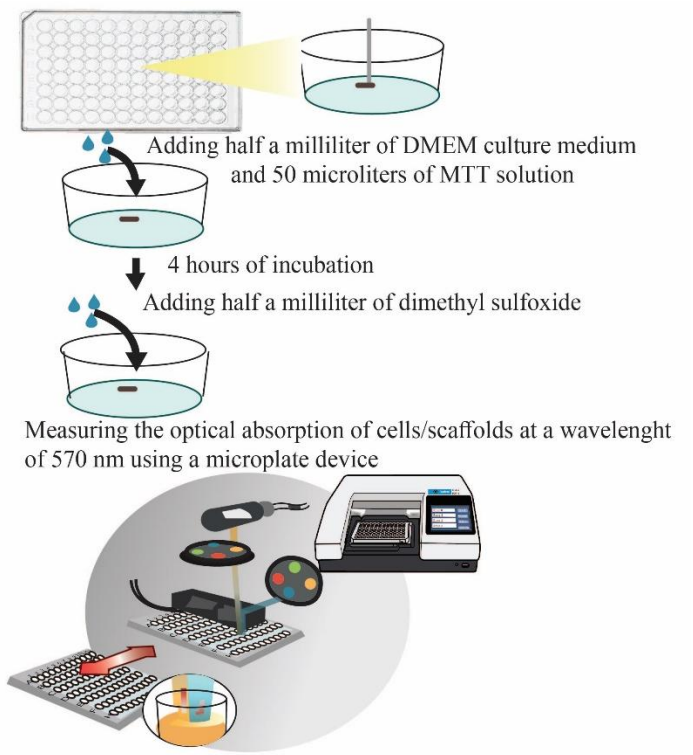

Figure 4. Microplate reader measurement of cell viability using the MTT assay at 570 nm [11].

In the MTT microplate assay, only a single type of nanoparticle, denoted as B, was tested in triplicate on the MCF-7 breast cancer cell line. The experimental workflow is illustrated in Figure 5.

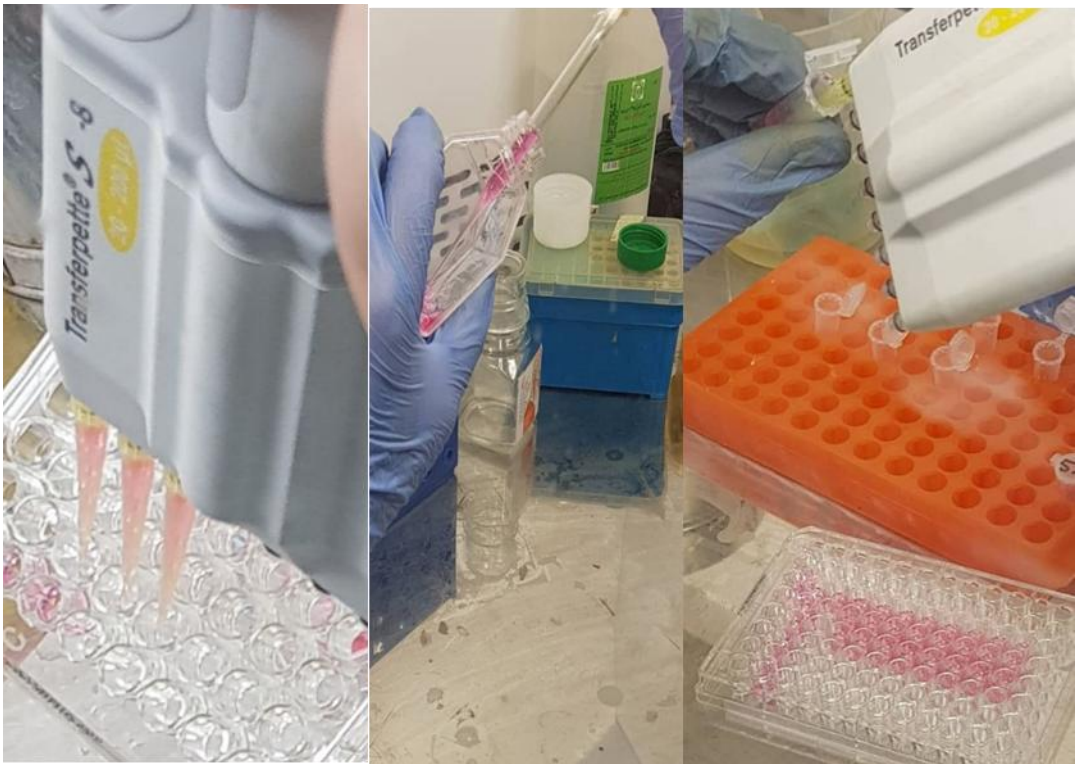

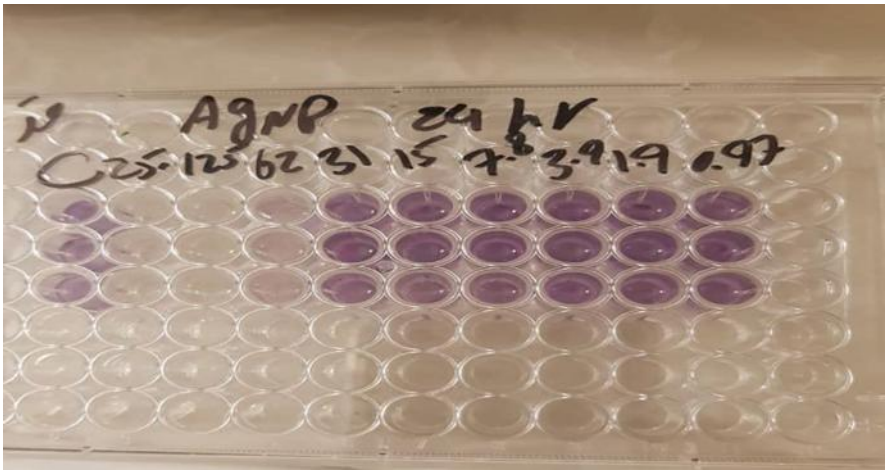

Figure 5. Workflow of the MTT assay in the present study.

2.5 Supplementary Experiments

2.5.1. Scanning Electron Microscopy (SEM)

The surface morphology of selected samples was examined using a scanning electron microscope (SEM), model PC3-WDX [30].

2.5.2 X-ray Diffraction (XRD)

X-ray diffraction (XRD) is a critical technique for the direct determination of phase types and crystalline structures of materials. In this study, a LabX XRD-6100 instrument was used [31].

2.5.3 Fourier-Transform Infrared Spectroscopy (FT-IR)

FT-IR analysis was employed to study the functional groups of the Tetra–AgNP nanocomposites using a Perkin Elmer Smart UAIR-two instrument. FT-IR spectra of AgNPs and Tetra–AgNPs were recorded in the range of 400–4000 cm^{-1} with a resolution of 4 cm^{-1}

2.5.4 Transmission Electron Microscopy (TEM)

TEM images were obtained using a Hitachi H-7100 microscope operating at accelerating voltages of 80 and 200 kV.

2.5.5 Evaluation of Antimicrobial Activity

The antibacterial activity of silver nanoparticles was assessed using the minimum inhibitory concentration (MIC) method. The bacterial strains used in this study included Staphylococcus aureus (ATCC 6538), Bacillus cereus (ATCC 14579), Escherichia coli (ATCC 25922), and Pseudomonas aeruginosa (ATCC 15442).

Briefly, primary bacterial cultures were prepared, and after 24 hours of growth, a 0.5 McFarland suspension (~1×10^7 CFU/mL) was obtained from the microbial culture medium. The MIC assay was performed according to CLSI standards using the microdilution method in 96-well microplates with three replicates. The concentration range for the extracts was 25–100 µg/mL [32].

For MIC determination, attention was paid to the orientation of the 96-well plate, with one side labeled with letters (A, B, …) to ensure consistent reading with an ELISA reader. In the first step, 1 mg of the respective nanoparticle was weighed using a four-decimal balance, placed into a microtube, and 1000 µL of Mueller-Hinton broth was added. The placement of samples within each plate consisted of eight rows, with nanoparticles A and B distributed across two to four rows per type.

The microtubes containing nanoparticles and broth were vortexed thoroughly. Using a micropipette, 100 µL of the mixture was added to the first well, with repeated pipetting to ensure proper mixing. Subsequent serial dilutions were performed across the remaining wells, transferring from well 1 to well 2, and so on, until the eighth well, where the final 100 µL was discarded. This ensured that nanoparticles were present in all wells.

Next, bacterial suspensions were added so that each row of four wells contained the same bacterial strain. Figure 6 illustrates the final MIC setup [2], [33].

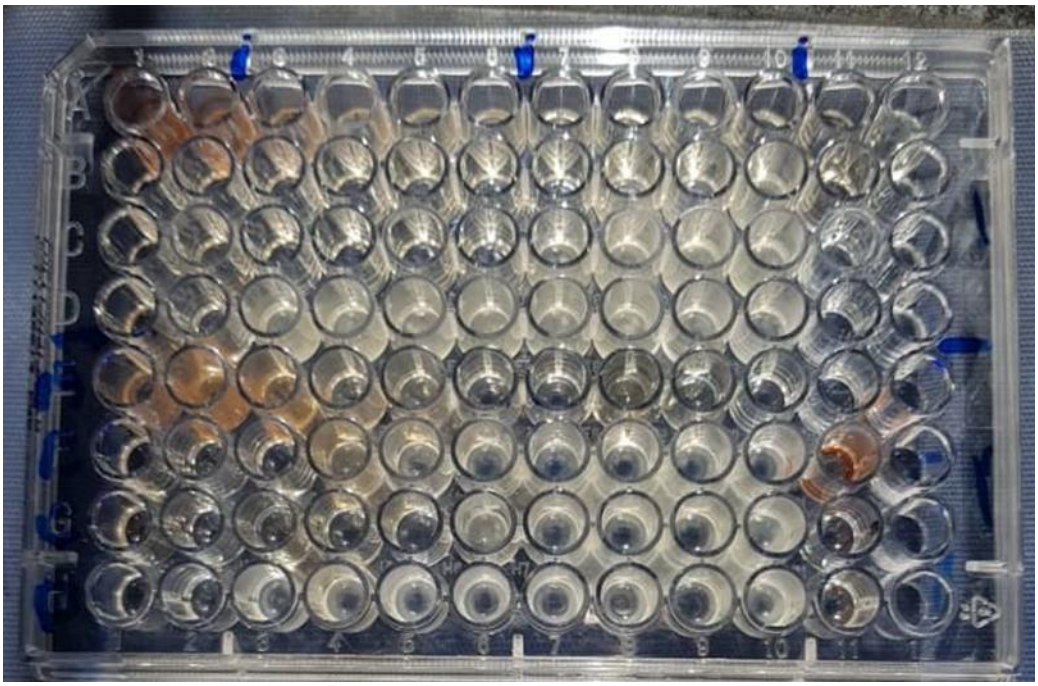

Figure 6. Final setup of the MIC assay.

2.6 Data Analysis

The collected data were analyzed using Origin software. In this study, all experiments were conducted in three separate sessions, with each session including three replicates.

3. Results and Discussion

3.1 Morphology of Silver Nanoparticles with Tetracycline

To investigate the morphology, each sample was examined separately using scanning electron microscopy (SEM) and transmission electron microscopy (TEM).

3.1.1 . Analysis of Sample A

Sample A corresponds to the root extract of Iris persica in an aqueous solution. Figure 7 presents TEM and SEM images at various magnifications of silver nanoparticles loaded with tetracycline, synthesized using the root extract in an aqueous medium. SEM results indicate that the synthesized nanoparticles exhibit a uniform, isotropic morphology. Particle size analysis revealed that the A-treated samples had an average grain size of 63.78 nm [34].

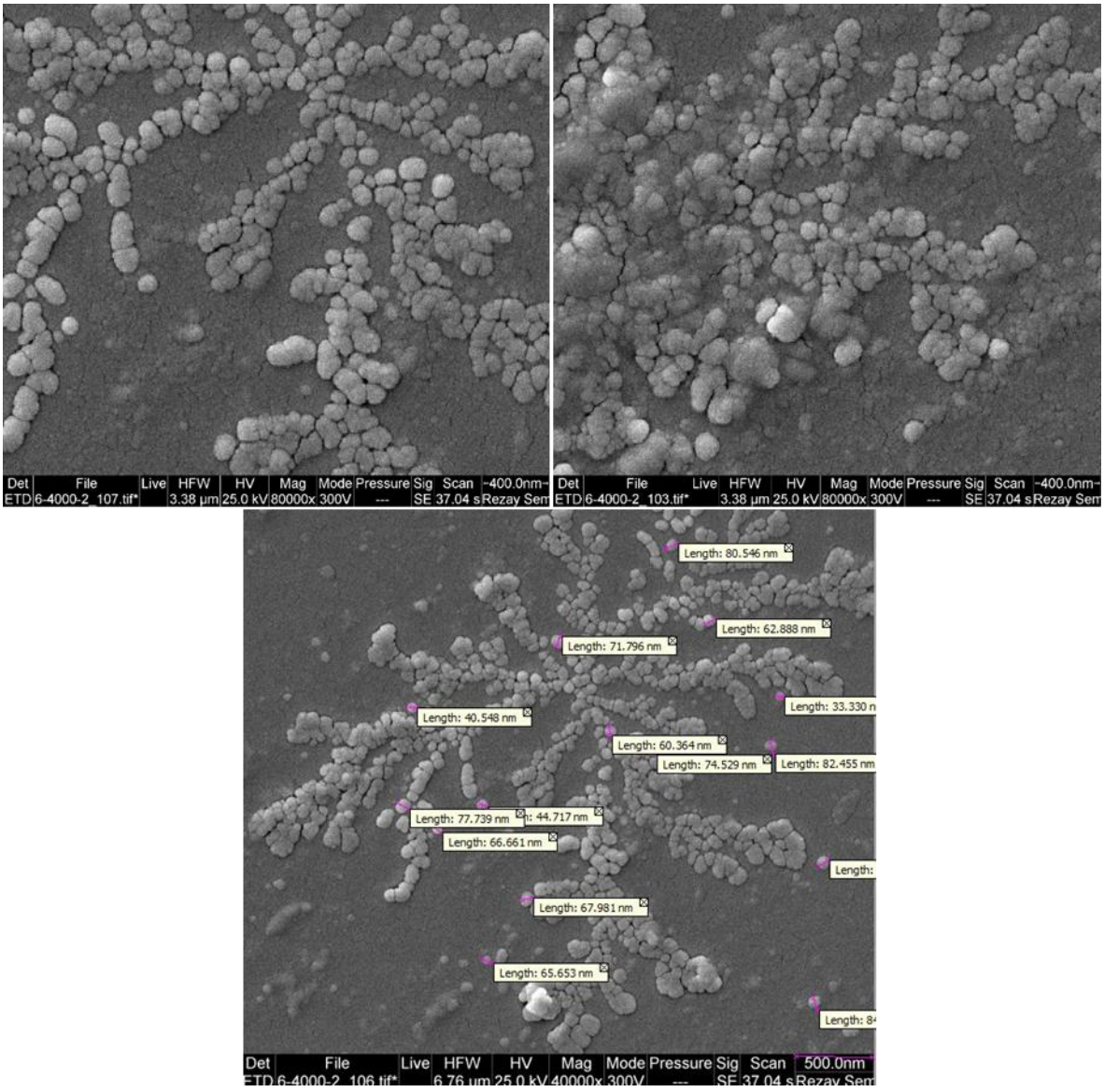

Figure 7. Scanning electron microscopy (SEM) images of silver nanoparticles loaded with tetracycline for treatment A

Figure 8 corresponds to transmission electron microscopy (TEM) images of silver nanoparticles loaded with tetracycline for treatment A. TEM results indicate that the synthesized nanoparticles exhibit a uniform, isotropic morphology, confirming the observations obtained from scanning electron microscopy (SEM). However, TEM analysis and the histogram curve presented in Figure 9 reveal that the particle sizes of the silver nanoparticles with tetracycline are smaller than those measured by SEM. The histogram and TEM results show that most particles fall within the 0–45 nm range, indicating that the particle size is smaller than 63.78 nm. Calculations indicate an average particle size of 14.75 nm, and this discrepancy can be attributed to the agglomeration of silver nanoparticles with tetracycline observed in the SEM images [3].

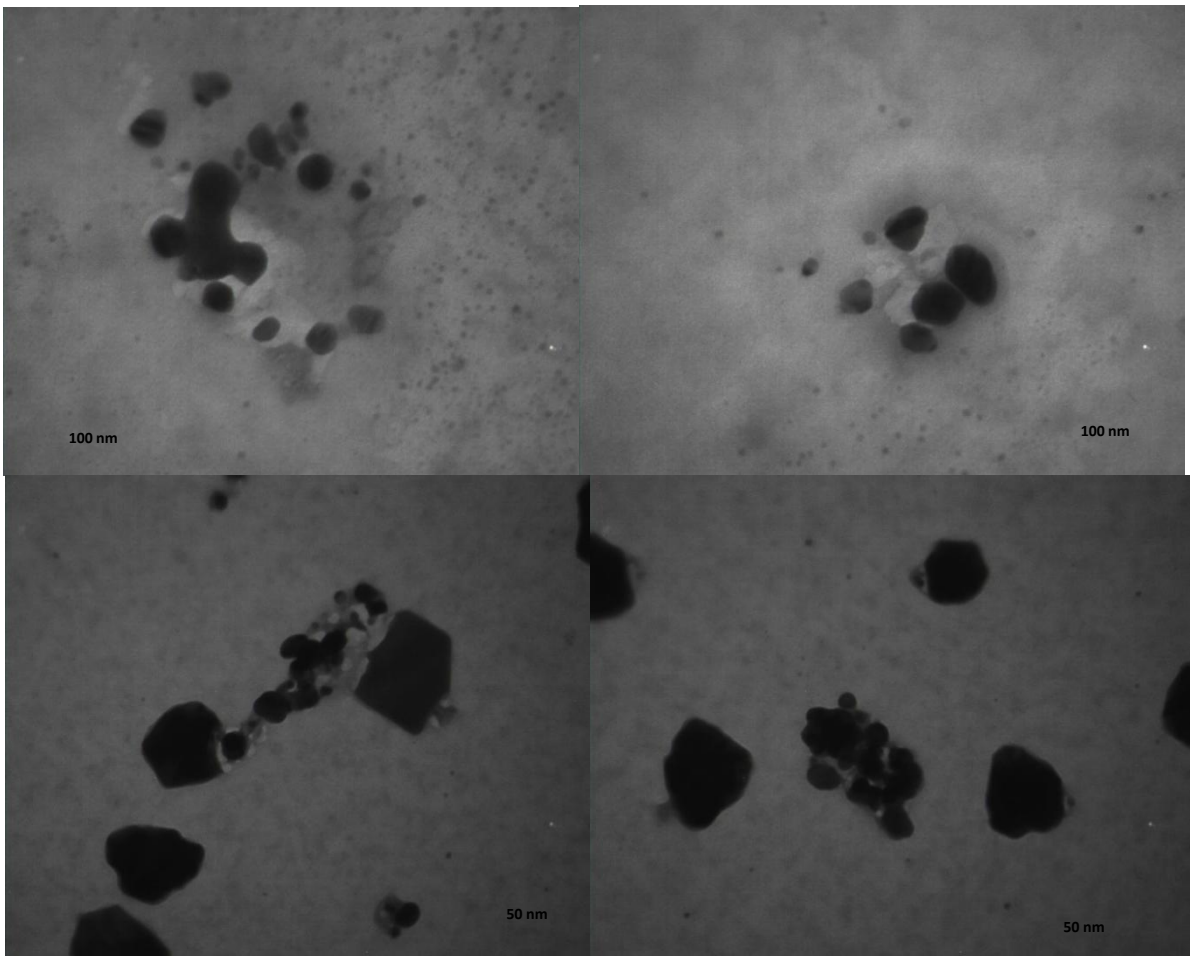

Figure 8. Transmission electron microscopy (TEM) image of silver nanoparticles loaded with tetracycline for treatment A.

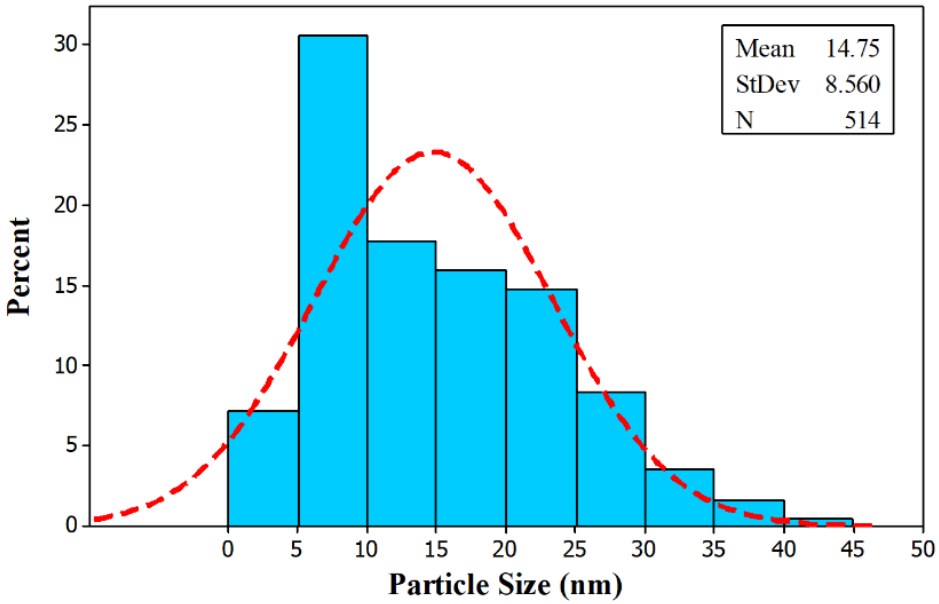

Figure 9. Histogram of silver nanoparticles loaded with tetracycline synthesized for treatment A.

Energy-dispersive X-ray spectroscopy (EDS) results for the sample synthesized under treatment A. The analysis indicates that approximately 12% of the composition corresponds to silver, with the remainder being oxygen. The presence of oxygen is attributed to the voids between the nanoparticles. Overall, these results confirm the formation of silver nanoparticles loaded with tetracycline [30].

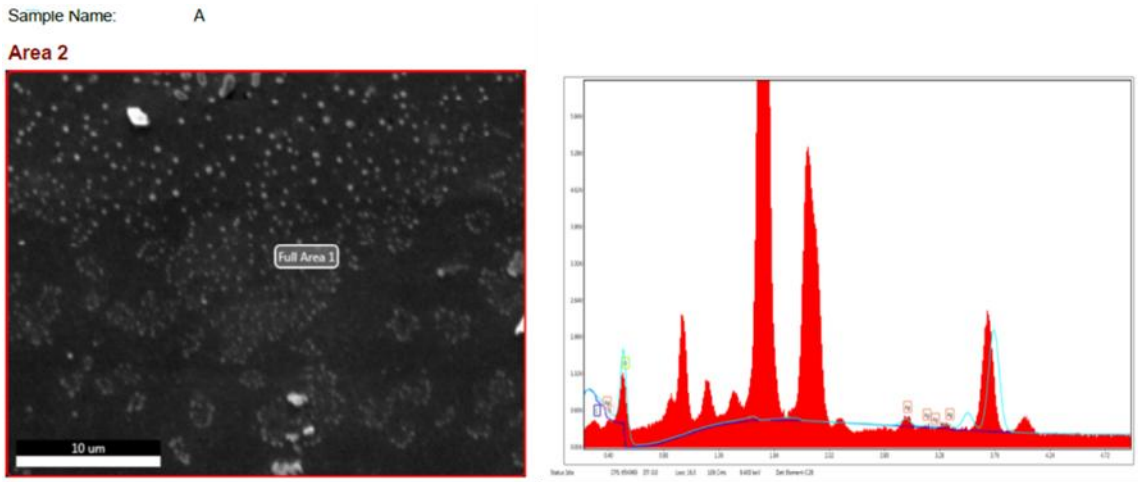

Figure 10. EDS results for nanoparticles synthesized under treatment A.

The X-ray diffraction (XRD) pattern of silver nanoparticles synthesized using Iris plant extract is presented, showing peaks at (111), (200), (220), and (311) with 2θ values of 38.07°, 44.26°, 67.33°, and 77.35°, respectively, corresponding to the face-centered cubic (FCC) structure of silver nanoparticles loaded with tetracycline. These results are in complete agreement with the standard XRD pattern of silver. The narrow width of the diffraction peak at half maximum of the (111) reflection indicates a relatively large crystalline size of the tetracycline-loaded silver nanoparticles. These findings are consistent with those reported by Samer and colleagues [30].

Table 1 eZAF Smart Quant Results

Element	Net Intensity	Atomic %	Weight %
C (CK)	0	0	0
N (NK)	0.03	0.02	0.01
O (OK)	526.71	97.93	87.59
Ag (AaL)	86.97	2.06	12.40

Figure 11 illustrates the FTIR spectra for the silver nanoparticles loaded with tetracycline (Figure 11a) and for the plant extract sample (Figure 11b). The FTIR spectral analysis was conducted to identify the biomolecular functional groups responsible for stabilizing and capping the synthesized tetracycline-loaded silver nanoparticles.

In the spectrum, the peaks observed at 3359–3398 cm^{-1} correspond to NH stretching vibrations, while the peaks at 2922–2924 cm^{-1} are attributed to CH stretching. The peaks at 1632–1638 cm^{-1} are associated with amino acids containing NH_2 groups, and the amine I bond is observed at 1401–1415 cm^{-1}, reflecting changes in C–H stretching. Carbonyl and ester groups appear at 1147–1154 cm^{-1}, related to skeletal stretching of C–O bonds, while peaks at 1019–1021 cm^{-1} correspond to P–O stretching vibrations.

These data indicate that amide, carboxyl, amine, and residual amino acid groups present in the iris root extract play a crucial role in the synthesis and stabilization of tetracycline-loaded silver nanoparticles [35].

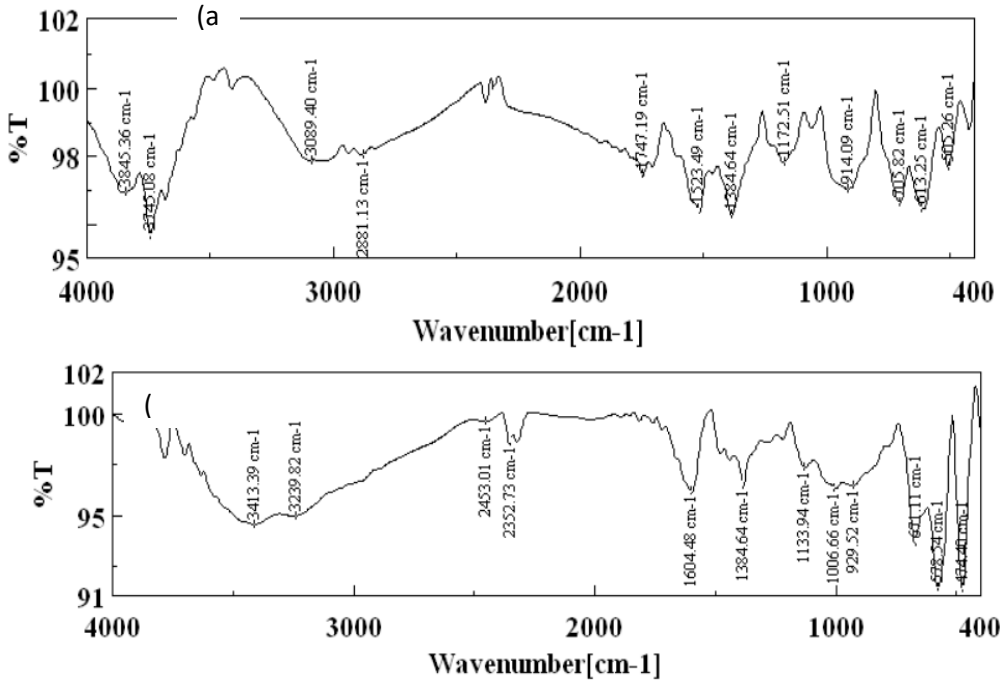

Figure 11. FTIR spectra for treatment A: (a) tetracycline-loaded silver nanoparticles, (b) plant extract.

3.1.2 Examination of Sample B

Sample B corresponds to the root extract of Iris persica in an aqueous solution. Figure 12 shows various magnifications of tetracycline-loaded silver nanoparticles synthesized using the aerial parts of Iris persica in an aqueous medium. The results obtained from scanning electron microscopy (SEM) indicate that the synthesized particles exhibit a roughly spherical morphology. Particle size measurements show that the nanoparticles in treatment B have an average diameter of 23.58 nm.

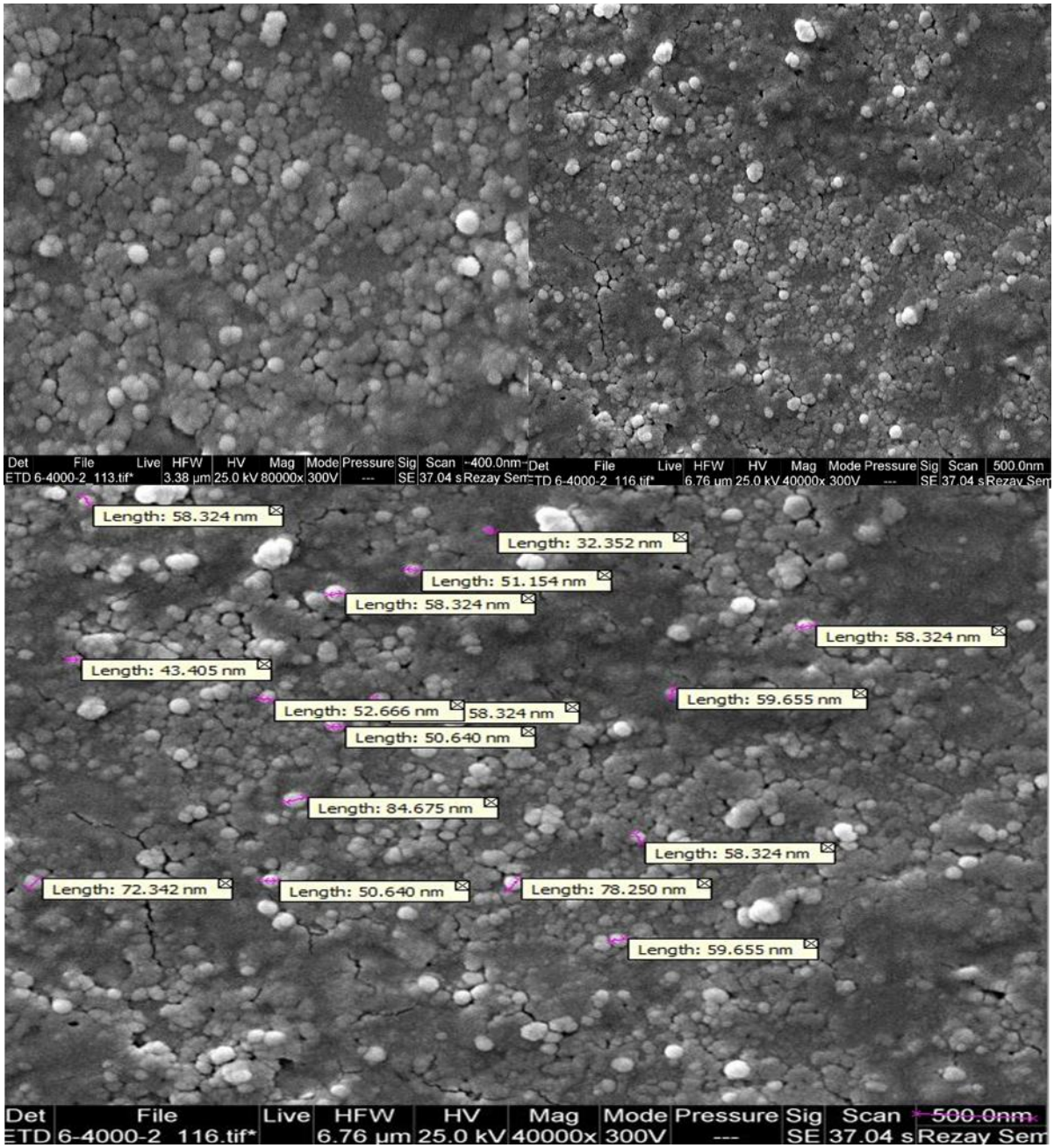

Figure 12. Scanning electron microscopy (SEM) image of tetracycline-loaded silver nanoparticles for treatment B.

The results obtained from scanning electron microscopy (SEM) indicate that the synthesized particles exhibit a roughly spherical morphology. Particle size measurements reveal that the nanoparticles in treatment A have an average diameter of 78.63 nm.

Figure 13 corresponds to the transmission electron microscopy (TEM) analysis of silver nanoparticles for treatment B. TEM results show that the tetracycline-loaded nanoparticles also possess a roughly spherical morphology, corroborating the SEM observations. However, TEM analysis and the histogram curve presented in Figure 14 reveal that the particle size of the tetracycline-loaded silver nanoparticles is smaller than that measured by SEM. Data from the histogram and TEM indicate that the majority of particles range from 0 to 45 nm, which is below the average size of 23.58 nm reported for SEM measurements. Calculations indicate an average particle size of 15.61 nm, and this discrepancy is attributed to the agglomeration of tetracycline-loaded silver nanoparticles under SEM conditions [36].

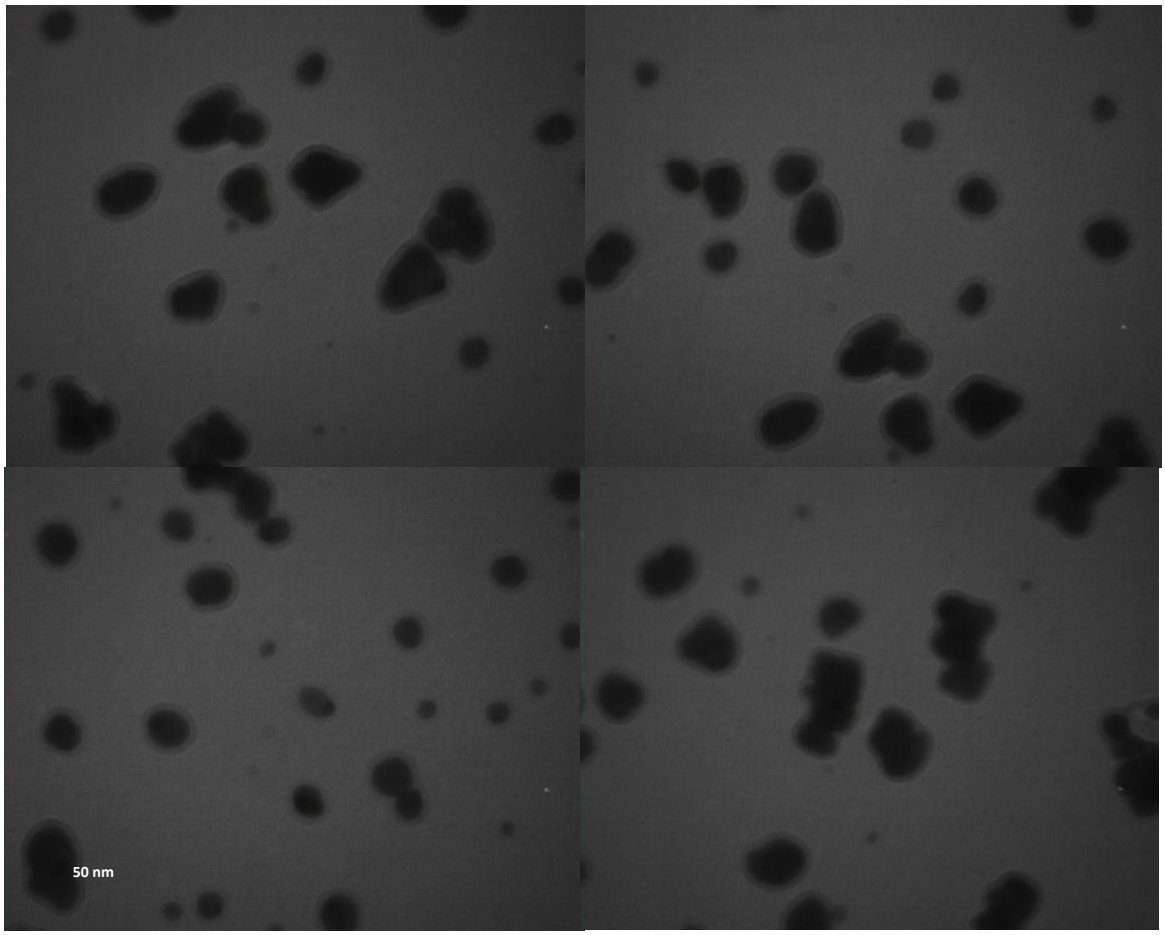

Figure 13 – Transmission electron microscopy (TEM) image of silver nanoparticles for treatment B.

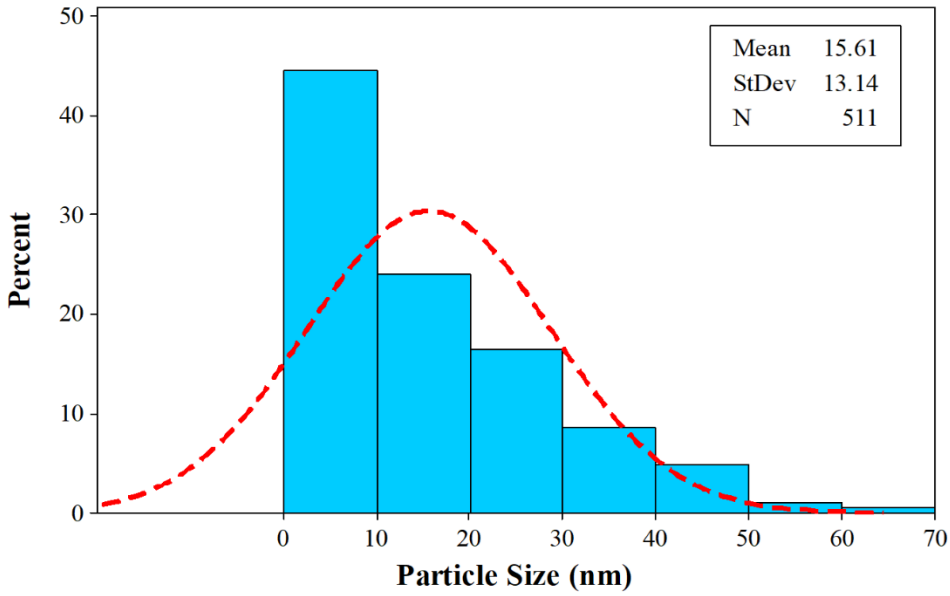

Figure 14. Histogram curve of tetracycline-loaded silver nanoparticles synthesized under treatment B.

Figure 15 illustrates the EDS results for the sample synthesized under treatment B. The analysis indicates that approximately 17.74% of the sample is composed of silver, while the remaining portion consists of oxygen. The presence of oxygen can be attributed to the voids between the particles on the substrate. Overall, these results confirm the successful synthesis of tetracycline-loaded silver nanoparticles.

Additionally, the SEM observations indicate that the synthesized particles exhibit a coaxial morphology. Particle size measurements reveal that the samples under treatment B have an average grain size of 23.58 nm. TEM analysis and the corresponding histogram demonstrate that the majority of the synthesized nanoparticles fall within the 0–45 nm range, indicating that the particle size is smaller than the SEM-determined value. Calculations yield an average size of 15.61 nm, which can be attributed to the agglomeration of silver nanoparticles in the SEM imaging conditions.

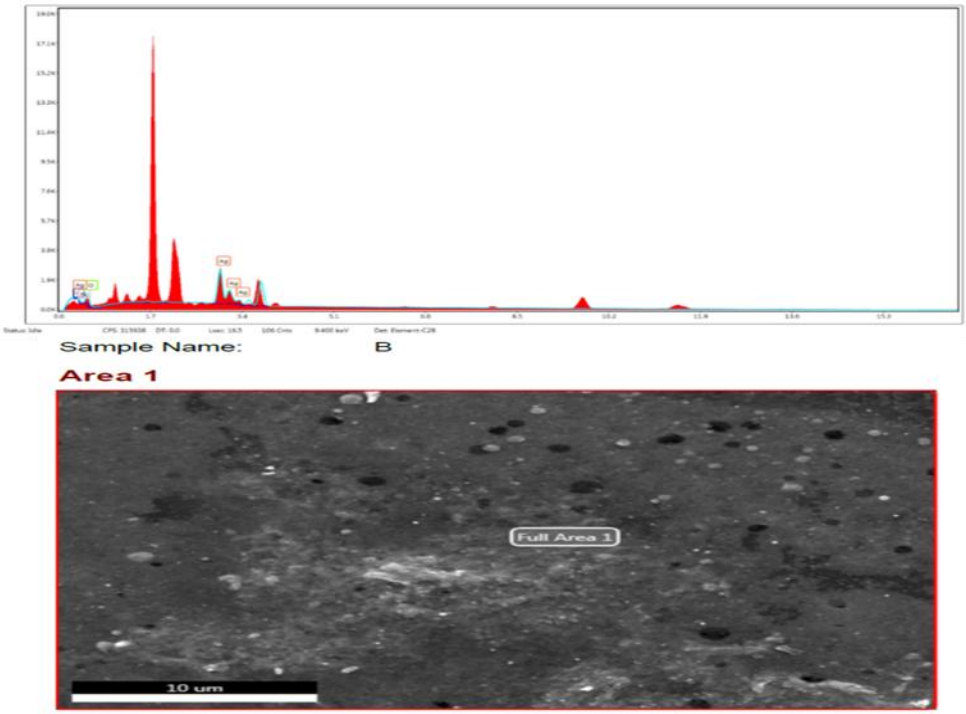

Figure 15. EDS results for tetracycline-loaded silver nanoparticles synthesized under treatment B.

Table 2 eZAF Smart Quant Results for Treatment B

Element	Net Intensity	Atomic %	Weight %
C (Carbon)	0	0	0
N (Nitrogen)	0.06	0.02	0.01
O (Oxygen)	266.41	82.25	40.75
Ag (Silver)	1453.09	17.74	59.25

Figure 16 presents the FTIR spectra for the silver nanoparticles with tetracycline (Figure 16a) and the plant extract sample (Figure 16b). FTIR spectral analysis was performed to identify the biomolecules responsible for acting as capping agents in the synthesis of silver nanoparticles with tetracycline [37]. The nanoparticle sample is shown in Figure 16. In this spectrum, peaks observed at 3359–3398 cm^{-1} correspond to NH bonds, those at 2922–2924 cm^{-1} are attributed to CH bonds of amides, peaks at 1632–1638 cm^{-1} are associated with amino acids containing NH_2 groups, and peaks at 1401–1415 cm^{-1} are assigned to type I amine groups due to C–H deformation. Furthermore, peaks at 1147–1154 cm^{-1} correspond to skeletal stretching of dimethyl groups, while those at 1019–1021 cm^{-1} are attributed to P–O stretching vibrations. These results indicate that amide, carboxyl, amino, and residual amino acid groups present in the aerial parts of the plant extract in the aqueous solution play a significant role in the synthesis of silver nanoparticles with tetracycline [31].

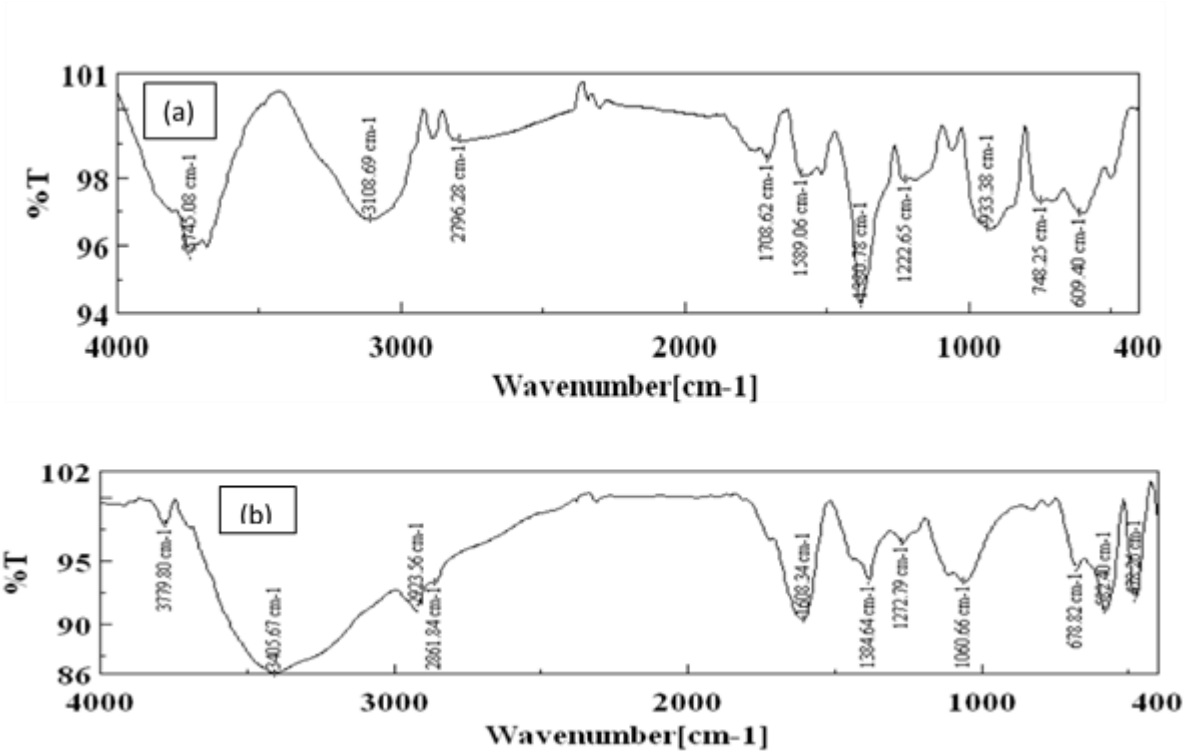

Figure 16. FTIR spectra of Treatment B: (a) silver nanoparticles synthesized with tetracycline, (b) aqueous plant extract.

3.2. Antimicrobial Properties of Silver Nanoparticles (MIC)

The results related to the antibacterial activity of silver nanoparticles synthesized with tetracycline via the biosynthesis method using Treatments A and B are summarized in Tables 1–4 [38, 39].

Table 3 Microbiological results for the sample under Treatment A

Bacterial Strain	0.2	0.1	0.05	0.025	0.0125
Escherichia coli DH5α, K12, ATCC35218 (E1, E4, E5, E6, E8, E9)	–	–	–	–	+
Bacillus cereus ATCC9634 (E2, E3, E7, E-IMP)	–	–	+	+	+
Pseudomonas aeruginosa (BAL strain, S2), *Staphylococcus aureus* ATCC25923, *Enterococcus faecalis* ATCC29212 (S1, S3)	–	+	+	+	+

Abbreviations for Table 3: E1–E9: Escherichia coli BAL strains numbered 1 to 9. E-IMP: BAL strains of Escherichia coli producing metallo-β-lactamase. S1–S3, IMP: Staphylococcus aureus BAL strains numbered 1 to 3. Symbols: "–" indicates no bacterial growth, while "+" indicates bacterial growth.

Table 4. Measurement of MIC and MBC values for Treatment A

Silver Nanoparticle Concentration (mM)	MIC (mm)	MBC (Log CFU/ml)
0	0	6.7
0.0125	3	6.6
0.025	5	5.9
0.05	6	5.5
0.1	8	4.8
0.2	8	3.9

Table 5 . Microbiological results for Treatment B

Bacterial Strain	**Silver Nanoparticle Concentration (mM)**	**0.2**	**0.1**	**0.05**	**0.025**	**0.0125**
Escherichia coli DH5α, K12, ATCC35218	E1, E4–E9	-	-	-	+	+
Bacillus cereus ATCC9634	E-IMP, E2, E3, E7	-	-	+	+	+
Pseudomonas aeruginosa (clinical strain), S2	—	+	+	+	+	+
Staphylococcus aureus ATCC25923, *Enterococcus faecalis* ATCC29212	S1–S3	?	+	+	+	+

- E1–E9: Escherichia coli strains numbered 1 to 9.
- E-IMP: Clinical E. coli strains producing metallo-β-lactamase.
- S1–S3: Numbered clinical Staphylococcus aureus strains 1 to 3.
- "–" indicates absence of bacterial growth.
- "+" indicates presence of bacterial growth.

Table 6. Measurement of MIC and MBC Values for Treatment B

MBC (Log CFU/mL)	**MIC (mm)**	**Silver Nanoparticle Concentration (mM)**
6.7	0	0
6.4	3	0.0125
5.6	5	0.025
4.8	6	0.05
3.5	8	0.1
2.7	8	0.2

Antibacterial and antifungal properties of Iranian Iris have been reported in numerous studies. These investigations have demonstrated, in addition to inhibitory effects against human pathogenic microbes, significant activity against certain plant and animal pathogens as well as food spoilage agents. However, to date, no study has evaluated the effects of nanoparticles synthesized using extracts of this plant [40].

Bacteria responsible for hospital-acquired infections have shown high sensitivity to Iranian Iris, and depending on the microbial species and the concentration of the essential oil or plant extract, the effects can be bacteriostatic or bactericidal. In these studies, the essential oil of Iranian Iris was tested against pathogenic bacteria including Bacillus anthracis, Escherichia coli, Helicobacter pylori, Klebsiella pneumoniae, and Staphylococcus aureus. The Iranian Iris exhibited inhibitory effects against all tested organisms. The researchers suggested that Iranian Iris, either alone or in combination with other antibiotics, may be useful in the prevention or treatment of severe infections, particularly those that are difficult to treat or antibiotic-resistant. These findings are consistent with the results of Tuba Unver and colleagues, who, through screening of phenolic compounds and evaluating the antimicrobial properties of Iranian Iris (Iris persica L. subsp. persica) extracts using in vitro and in silico methods, reported similar antimicrobial activity [29].

4. Conclusion

This study successfully synthesized and characterized silver nanoparticles (AgNPs) functionalized with tetracycline (Tetra–AgNP) using a biogenic approach, and evaluated their physicochemical, antimicrobial, and cytotoxic properties. Characterization via X-ray diffraction (XRD), scanning electron microscopy (SEM), transmission electron microscopy (TEM), energy-dispersive X-ray spectroscopy (EDS), and Fourier-transform infrared spectroscopy (FTIR) confirmed the formation of well-defined nanoparticles with an average size of approximately 63.78 nm. FTIR analysis revealed the presence of functional groups derived from both tetracycline and the plant extract, indicating effective capping and stabilization of nanoparticles, which is crucial for their biological activity.

The antimicrobial assessment demonstrated that Tetra–AgNPs exhibited significant antibacterial effects against multiple strains of pathogenic bacteria, including Escherichia coli, Bacillus cereus, Staphylococcus aureus, Pseudomonas aeruginosa, and Enterococcus faecalis. The measured minimum inhibitory concentrations (MIC) and minimum bactericidal concentrations (MBC) indicated that the nanoparticles were effective even at relatively low concentrations, highlighting their potential as alternative or adjunct antimicrobial agents. These findings align with previous reports on the antibacterial and antifungal properties of Iris persica extract, suggesting a synergistic effect between the plant-derived compounds and silver nanoparticles.

Cytotoxicity evaluations further demonstrated that Tetra–AgNPs possess favorable biocompatibility, indicating their safety for potential biomedical applications, particularly in drug delivery systems. The combined evidence suggests that these nanoparticles could provide an effective, environmentally friendly, and biocompatible platform for antimicrobial therapy, addressing challenges posed by antibiotic-resistant pathogens.

However, certain limitations must be considered. The study focused primarily on in vitro antimicrobial and cytotoxic assessments, and in vivo evaluations are necessary to fully understand the pharmacokinetics, biodistribution, and long-term safety of these nanocomposites. Additionally, the mechanistic pathways underlying the observed antimicrobial effects require further elucidation to optimize nanoparticle design and functionality.

Future research should explore large-scale synthesis methods, investigate synergistic interactions with conventional antibiotics, and evaluate the efficacy of Tetra–AgNPs in complex biological systems. Moreover, exploring their potential applications in food preservation, agricultural pathogen control, and targeted drug delivery could expand the utility of these nanocomposites.

In conclusion, this study demonstrates that biogenically synthesized Tetra–AgNPs are well-characterized, biologically active, and biocompatible, offering promising potential for antimicrobial applications. The integration of plant-derived compounds with nanotechnology represents a significant step toward developing safe and effective strategies to combat microbial infections and antibiotic resistance, reinforcing the importance of this research in advancing both nanomedicine and sustainable therapeutic approaches.

Funding: This research received no external funding.

Conflicts of Interest: The authors declare no conflict of interest.

Publisher's Note: All claims expressed in this article are solely those of the authors and do not necessarily represent those of their affiliated organizations, or those of the publisher, the editors and the reviewers.

References

[1] Y. Charles, "Nanoparticles with Raman Spectroscopic Fingerprints for DNA and RNA Detection," vol. 1536, no. 2002, 2012, doi: 10.1126/science.297.5586.1536.

[2] K. P. Steckiewicz et al., "Silver Nanoparticles as Chlorhexidine and Metronidazole Drug Delivery Platforms : Their Potential Use in Treating Periodontitis Silver Nanoparticles as Chlorhexidine and Metronidazole Drug Delivery Platforms : Their Potential Use in Treating Periodontitis," 2023, doi: 10.2147/IJN.S339046.

[3] S. Nikolova et al., "Drug-Delivery Silver Nanoparticles : A New Perspective for Phenindione as an Anticoagulant," pp. 1–26, 2023.

[4] G. S. S. N. Liposome-based and R. Analysis, "Nanoarchitectonics for Cancer Management : In Vitro Drug," 2023.

[5] S. Hussain and A. K. Pal, "Incorporation of nanocrystalline silver on carbon nanotubes by electrodeposition technique," vol. 62, pp. 1874–1877, 2008, doi: 10.1016/j.matlet.2007.10.021.

[6] K. Cho, J. Park, T. Osaka, and S. Park, "The study of antimicrobial activity and preservative effects of nanosilver ingredient," vol. 51, pp. 956–960, 2005, doi: 10.1016/j.electacta.2005.04.071.

[7] G. Caroling, E. Vinodhini, A. M. Ranjitham, and P. Shanthi, "Biosynthesis of Copper Nanoparticles Using Aqueous Phyllanthus Embilica (Gooseberry) Extract- Characterisation and Study of Antimicrobial Effects," vol. 63, no. 2, pp. 53–63, 2015.

[8] L. R. Jaidev and G. Narasimha, "Colloids and Surfaces B : Biointerfaces Fungal mediated biosynthesis of silver nanoparticles , characterization and antimicrobial activity," Colloids Surfaces B Biointerfaces, vol. 81, no. 2, pp. 430–433, 2010, doi: 10.1016/j.colsurfb.2010.07.033.

[9] A. Sati, T. N. Ranade, H. Khader, A. Yasin, and A. Pratap, "Silver Nanoparticles (AgNPs): Comprehensive Insights into Bio / Synthesis , Key Influencing Factors , Multifaceted Applications , and Toxicity A 2024 Update," 2025, doi: 10.1021/acsomega.4c11045.

[10] A. Mandal and N. Das, "Silver Nanoparticles as Drug Delivery Vehicle against Infections," no. July 2005, 2018, doi: 10.1080/10611860500233306.

[11] H. I. O. Gomes, C. S. M. Martins, and J. A. V. Prior, "Silver nanoparticles as carriers of anticancer drugs for efficient target treatment of cancer cells," Nanomaterials, vol. 11, no. 4, 2021, doi: 10.3390/nano11040964.

[12] C. G. Kumar and S. K. Mamidyala, "Colloids and Surfaces B : Biointerfaces Extracellular synthesis of silver nanoparticles using culture supernatant of Pseudomonas aeruginosa," Colloids Surfaces B Biointerfaces, vol. 84, no. 2, pp. 462–466, 2011, doi: 10.1016/j.colsurfb.2011.01.042.

[13] P. Mukherjee and S. Senapati, "Extracellular Synthesis of Gold Nanoparticles by the Fungus Fusarium oxysporum," no. 5, pp. 461–463, 2002.

[14] J. N. R. Ramji and H. S. P. Gautam, "Synthesis , stabilisation and characterisation of rhamnolipid-capped ZnS nanoparticles in aqueous medium," no. June 2009, 2010, doi: 10.1049/iet-nbt.2009.0010.

[15] K. Roy, C. K. Sarkar, and C. K. Ghosh, "Fast colourimetric detection of H 2 O 2 by biogenic silver nanoparticles synthesised using Benincasa hispida fruit extract," vol. 5, no. 2, pp. 251–258, 2016, doi: 10.1515/ntrev-2015-0054.
[16] P. Peter, "Multi-Functional Silver Nanoparticles for Drug Delivery : A Review," no. May, 2017.
[17] S. Sadhasivam, P. Shanmugam, and K. Yun, "Colloids and Surfaces B : Biointerfaces Biosynthesis of silver nanoparticles by Streptomyces hygroscopicus and antimicrobial activity against medically important pathogenic microorganisms," Colloids Surfaces B Biointerfaces, vol. 81, no. 1, pp. 358–362, 2010, doi: 10.1016/j.colsurfb.2010.07.036.
[18] G. Sajjadi, J. Amini, A. S. Arani, and H. Nezammahalleh, "Extracellular synthesis of silver nanoparticles using four fungal species isolated from lichens," 2017, doi: 10.1049/iet-nbt.2017.0170.
[19] M. Tiwari et al., "Biosynthesis of copper nanoparticles using copper-resistant Bacillus cereus, a soil isolate," Process Biochem., 2016, doi: 10.1016/j.procbio.2016.08.008.
[20] I. Medina-ramirez, Z. Luo, S. Bashir, and J. Louise, "Facile design and nanostructural evaluation of silver-modified titania used as disinfectant," pp. 1047–1054, 2011, doi: 10.1039/c0dt00784f.
[21] R. Nithya and R. Ragunathan, "SYNTHESIS OF SILVER NANOPARTICLE USING PLEUROTUS SAJOR CAJU AND ITS ANTIMICROBIAL STUDY," vol. 4, no. 4, pp. 623–629, 2009.
[22] Z. Sobhani, S. M. Samani, H. Montaseri, and E. Khezri, "Nanoparticles of chitosan loaded ciprofloxacin: Fabrication and antimicrobial activity," Adv. Pharm. Bull., vol. 7, no. 3, pp. 427–432, 2017, doi: 10.15171/apb.2017.051.
[23] M. J. Akhtar, M. Ahamed, S. Kumar, M. A. M. Khan, J. Ahmad, and S. A. Alrokayan, "Zinc oxide nanoparticles selectively induce apoptosis in human cancer cells through reactive oxygen species Zinc oxide nanoparticles selectively induce apoptosis in human cancer cells through reactive oxygen species," 2012, doi: 10.2147/IJN.S29129.
[24] C. Nmr, "C 60 in Water : Nanocrystal Formation and Microbial Response," pp. 4307–4316, 2007.
[25] G. L. Jones, C. T. Muller, M. O. Reilly, and D. J. Stickler, "Effect of triclosan on the development of bacterial biofilms by urinary tract pathogens on urinary catheters," no. December 2005, pp. 266–272, 2006, doi: 10.1093/jac/dki447.
[26] F. Paladini and M. Pollini, "Antimicrobial silver nanoparticles for wound healing application: Progress and future trends," Materials (Basel)., vol. 12, no. 16, 2019, doi: 10.3390/ma12162540.
[27] C. Petrarca et al., "Engineered metal based nanoparticles and innate immunity," Clin. Mol. Allergy, vol. 13, no. 1, pp. 1–12, 2015, doi: 10.1186/s12948-015-0020-1.
[28] H. J. Kim, H. R. Pant, A. Amarjargal, and C. S. Kim, "Incorporation of silver-loaded ZnO rods into electrospun nylon-6 spider-web-like nanofibrous mat using hydrothermal process," Colloids Surfaces A Physicochem. Eng. Asp., vol. 434, pp. 49–55, 2013, doi: 10.1016/j.colsurfa.2013.05.038.
[29] T. Unver, H. Uslu, I. Gurhan, and B. Goktas, "Screening of phenolic components and antimicrobial properties of Iris persica L. subsp. persica extracts by in vitro and in silico methods," Food Sci. Nutr., no. May, pp. 6578–6594, 2024, doi: 10.1002/fsn3.4251.
[30] S. H. Hussein-Al-Ali, S. M. Abudoleh, Q. I. A. Abualassal, Z. Abudayeh, Y. Aldalahmah, and M. Z. Hussein, "Preparation and characterisation of ciprofloxacin-loaded silver nanoparticles for drug delivery," IET Nanobiotechnology, vol. 16, no. 3, pp. 92–101, 2022, doi: 10.1049/nbt2.12081.
[31] S. Garg and A. Garg, "Encapsulation of Curcumin in Silver Nanoparticle for Enhancement of Anticancer Drug Delivery," Int. J. Pharm. Sci. Res., vol. 9, no. 3, p. 1160, 2018, doi: 10.13040/IJPSR.0975-8232.9(3).1160-66.
[32] M. Maklakova et al., "Potential Antibiotic Resurgence: Consecutive Silver Nanoparticle Applications Gradually Increase Bacterial Susceptibility to Antibiotics," ACS Omega, 2025, doi: 10.1021/acsomega.4c09240.
[33] H. H. Lara, N. V. Ayala-Núñez, L. C. I. del Turrent, and C. R. Padilla, "Bactericidal effect of silver nanoparticles against multidrug-resistant bacteria," World J. Microbiol. Biotechnol., vol. 26, no. 4, pp. 615–621, 2010, doi: 10.1007/s11274-009-0211-3.
[34] K. Alaqad and T. A. Saleh, "Gold and Silver Nanoparticles: Synthesis Methods, Characterization Routes and Applications towards Drugs," J. Environ. Anal. Toxicol., vol. 6, no. 4, 2016, doi: 10.4172/2161-0525.1000384.
[35] P. Wang, T. H. Wu, and Y. Zhang, "Novel silver nanoparticle-enhanced fluorometric determination of trace tetracyclines in aqueous solutions," Talanta, vol. 146, pp. 175–180, 2016, doi: 10.1016/j.talanta.2015.07.065.
[36] N. Hussein et al., "Evaluation of the synergistic effects of synthesized silver nanoparticles conjugated tetracycline," Eng. Technol. J., vol. 42, no. 4, pp. 437–445, 2024, doi: 10.30684/etj.2024.147316.1706.
[37] A. Z. Hameed and N. N. Hussein, "Detection of antibiofilm formation by sliver nanoparticles created by tetracycline antibiotic," J. Phys. Conf. Ser., vol. 1879, no. 2, 2021, doi: 10.1088/1742-6596/1879/2/022035.
[38] P. Parvekar, J. Palaskar, S. Metgud, R. Maria, and S. Dutta, " The minimum inhibitory concentration (MIC) and minimum bactericidal concentration (MBC) of silver nanoparticles against Staphylococcus aureus ," Biomater. Investig. Dent., vol. 7, no. 1, pp. 105–109, 2020, doi: 10.1080/26415275.2020.1796674.
[39] E. D. Cavassin et al., "Comparison of methods to detect the in vitro activity of silver nanoparticles (AgNP) against multidrug resistant bacteria," J. Nanobiotechnology, vol. 13, no. 1, pp. 1–16, 2015, doi: 10.1186/s12951-015-0120-6.
[40] F. Faedmaleki, F. H. Shirazi, A. A. Salarian, H. A. Ashtiani, and H. Rastegar, "Toxicity effect of silver nanoparticles on mice liver primary cell culture and HepG2 cell line," Iran. J. Pharm. Res., vol. 13, no. 1, pp. 235–242, 2014.